

Evaluation Mappings of Spatial Accelerator Based On Data Placement

Wu Zhipeng, Liu Yu, *Member, IEEE*,

Abstract—The scheduling strategies of workloads are critical to fully exploiting the performance of spatial accelerators, accurate performance models are required to evaluate the mapping of workloads. Recent works proposed various cost-model to describe the dataflow of the spatial accelerator. However, they are less expressive about customized memory hierarchies and thus lead to inaccurate performance models. In this paper, we propose, PolyAcc, a framework for evaluating the mappings of workload on spatial accelerator based on data placement. The Data placement relation describes the temporal-spatial relation of data at different memory levels, which can accurately capture the runtime behavior of hardware units. Based on data placement relations, polyAcc accurately analyzes the data volume for different reuse patterns and estimate metrics, including data reuse, latency, and energy. Overall, polyAcc closely matches the ideal execution time and PE utilization for GEMM and Conv workloads, respectively achieves 0.82%, 18.8% improvements for execution time and energy consumption estimates in validation against Eyeriss architecture compared to the state-of-the-art framework.

Index Terms—Spatial Accelerator, Cost-Model, Polyhedral Model



1 INTRODUCTION

Spatial accelerators have emerged in the recent past to accelerate compute- and memory-intensive applications, such as data analysis, deep learning, due to their lower runtime and energy-efficiency. The main factor for the high efficiency of the spatial accelerators is that allocate dedicated memory to form customized memory hierarchies that ensure the compute engine is busy computing the data being fed, namely, the “right” data should be moved in or out the “right” locations at the “right” time-stamp. Programmers must manage critical data orchestration explicitly to precisely control when and where data is used. A primary current focus is how to estimate performance of mappings of workload on spatial accelerators.

To evaluate the performance of accelerators, Some recent works have been proposed various cost models. State-of-the-art techniques estimate performance and energy consumption using either compute-centric [1], [2], [3] or data-centric [4], or relation-centric [5]. However, both framework have some limitations. First, these analytical methods are less expressive, and they can only represent a subset of the topology of the accelerator, incomplete abstractions could hurt the accurate performance model. For example, failure to consider interconnections between hardware units limits data reuse analysis of compute-centric method. And, the previous work [4] assume a fixed accelerator architecture with a 2-level memory hierarchy, which limits the framework’s use. Second, both analytical methods fail to support accurate performance analysis. The compute-centric does not consider data transfer between PEs, and the data-centric and relation-centric ignore the impact of memory, leading to inaccurate performance estimates.

All of these limitations affect the quality of evaluating results and further impact the mapping decisions that designers derive based on these results. To overcome this challenge, in this paper, we propose a framework, PolyAcc, to estimate the performance and energy consumption of mappings on spatial architectures. We present a memory-centric representation to model the spatial accelerator, which is a hierarchical tree to describe various memory hierarchies and interconnections in the accelerator. We propose data placement relation (DPR) to capture the runtime behavior of data transfer between hardware units across space and time. Based on the DPR, performance metrics can be easily computed using polyhedral operations. Overall, polyAcc can estimate various hardware metrics, including data reuse, latency, PE utilization, and energy consumption. Results show that PolyAcc achieves accurate PE utilization estimates, 0.82% and 18.8% improvements in execution time and energy consumption estimates compared to the state-of-the-art framework. Overall, the contribution of the paper are:

- A memory-centric representation to model the spatial accelerator and mapping strategies.
- An analytical model for mapping workload on a spatial architecture with data placement relation.
- A closed-form analytical method to estimate workload execution time and energy.

The rest of the paper is organized as follows. Section 2 introduces the background of spatial accelerator and polyhedral model. Section 3 presents the PolyAcc framework. Section 4 presents experimental results. Finally, this paper is concluded in Section 5.

- Liu Yu was with the School of Microelectronics, Tianjin University, Tianjin, China, 300072.
E-mail: liuyu@tju.edu.cn
- Wu Zhipeng with Tianjin University.

2 BACKGROUND

2.1 Spatial Accelerator

The spatial accelerator is mainly composed of a set of processing elements (PE) and the interconnection between PEs. Each PE includes local scratchpad and arithmetic logic units (ALUs). Fig.1(a) shows the example of a spatial accelerator with output-stationary dataflow, which is composed of 4×4 PE array, a on-chip shared memory, and private register files for each PE. Each PE is connected to the PE to the left and below, which represent data communication between PEs.

Based on the complex memory hierarchy and connection relation of hardware unit in the spatial accelerators, there are three major patterns of data reuse: (1)*Temporal Reuse*: units access the same data set stored in themselves across time. (2)*Spatial Reuse*: multiple units access the same data set at the same time via multicast/broadcast connection (3)*Spatial-Temporal Reuse*: adjacent units with point-to-point connections access the same data set in a skewed schedule.

These reuse features must be considered when evaluating the mapping strategies for any algorithm running on spatial accelerators.

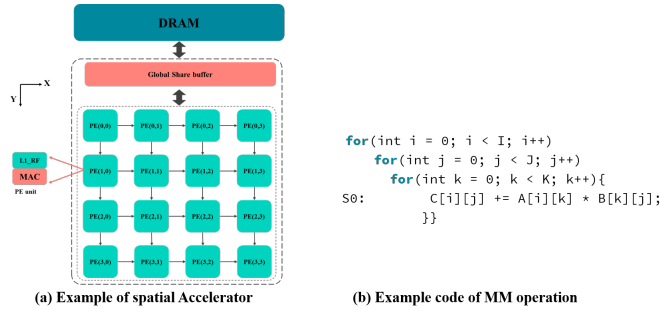


Fig. 1. Example of the Spatial Accelerator and MM operation. (a) shows an example of a spatial architecture with output-stationary dataflow, which has three levels of memory: DRAM, on-chip shared memory and private register files in PEs. (b) shows the example code of MM operator

2.2 Polyhedral Model

The polyhedral model is a powerful abstraction for analyzing and transforming loop nest programs. A program in the polyhedral model is typically represented by three items: iteration domain, access function, and a schedule. The matrix multiplication code shown in Fig.1(b) will be used to illustrate these concepts.

The iteration domain contains the loop instances of the statement in the program. The iteration domain of the loop in Fig.1(b) is defined as the following: $domain = \{S0[i, j, k] : 0 \leq i \leq I \wedge 0 \leq j \leq J \wedge 0 \leq k \leq K\}$, where $S0[i, j, k]$ is a loop instance and $0 \leq i \leq I \wedge 0 \leq j \leq J \wedge 0 \leq k \leq K$ gives the constraints.

The access function maps the statement instance to the array index, which includes read access function and write access function. The read access function in Fig.1(b) are shown below: $R = \{S0[i, j, k] \rightarrow C[i, j]; S0[i, j, k] \rightarrow B[k, j]; S0[i, j, k] \rightarrow A[i, k]\}$. The write access relation in the loop is: $W = \{S0[i, j, k] \rightarrow C[i, j]\}$. The access function means the loop instance $S0[i, j, k]$ access the array element $C[i, j]$, $B[k, j]$ and $A[i, k]$.

The schedule represents the lexicographical order of statement instances that leverages a multi-dimensional affine function. The schedule in Fig.1(b) are shown below: $Sch = \{S0[i, j, k] \rightarrow [i, j, k]\}$. The schedule can be explicitly encoded using a tree structure [6], which can simplify the modeling of automatic memory managements in polyhedral compilers.

In this work, we use the Integer Set Library [7] for performing polyhedral operations, and we use the same notation as used in ISL to elucidate the concepts and the algorithm. Table 2 lists the notation for polyhedral operations used in the article.

TABLE 1
The notation for Polyhedral operations used in the article

Notation	Interpretation
\circ	Two relations are composed to form a new relation.
R^{-1}	The relation R is inverted.
\cup	The union of two integer sets or relations.
\cap	The intersection of two integer sets or relations.
$Sum()$	Building a counting formula for an integer set or relation.

3 OVERVIEW OF POLYACC

In this section, we describe our framework, PolyAcc, for implementing mapping analysis for the spatial accelerator based on data placement. As shown in Fig.2, PolyAcc takes the specification of spatial architecture, the data partition and schedule strategies as input. Then, PolyAcc automatically constructs a scheduling tree including memory hierarchy information, which represents the lexicographical order of the workload. After that, PolyAcc scans the scheduling tree to infer each memory level's data placement relation. PolyAcc analyzes data reuse via data placement relations and obtains various performance metrics precisely, which can help designers explore the hardware design space and find the optimal mapping strategies.

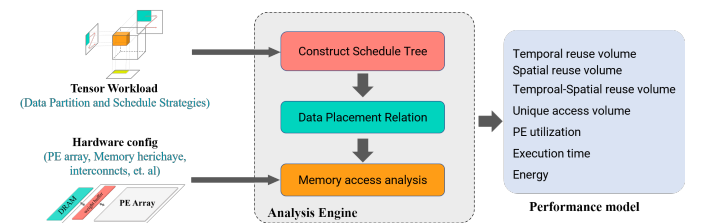


Fig. 2. PolyAcc Overview

3.1 Abstraction for Architecture and Mapping

PolyAcc uses memory-centric notations to describe the spatial accelerator, which is a hierarchical tree to abstraction like the previous work [1]. Fig.3(a) shows the abstract of the example spatial accelerator in Fig.1(a) using tree-like description. We introduce three attributes to represent the topology of interconnection. The first attribute, Dim indicates how the current memory level units are laid in the physical dimension, by default on the x-axis. The second attribute, Virtual, facilitates the description of the spatial mapping of data tile,

and the memory level with this attribute has no dedicated physical memory. The third attributes, Connect, defines the interconnection of units at the current memory level, we use the Presburger Relations to describe the connection as below:

$$connection = \{[\vec{s}_1] \rightarrow [\vec{s}_2]\} \quad (1)$$

where \vec{s}_1 and \vec{s}_2 denote the coordinate of the hardware units that are connected. The relation can represent connections within the same level of hardware or connections at different levels of hardware. As shown in Fig.3(a), the ifmap_spad in L1 level memory has connect relation attribute: $\{[x, y] \rightarrow [x, y - 1]\}$, which means that data in the ifmap_spad can be propagated down to the adjacent ifmap_spad.

```

{ arch: {
  L3: {
    dimension: 1,
    subunit: {
      shared_glb: { num: [1] }}
    V2: {
      dimension: 1,
      subunit: {
        NOC: { num: [1] }}
      L1: {
        dimension: 2,
        subunit: {
          ifmap_spad: {
            num: [4,4],
            dim: [X,Y],
            internect: [[ [x,y]->[x,y-1] ] ]},
          weights_spad: {
            num: [4,4],
            dim: [X,Y],
            internect: [[ [x,y]->[x-1,y] ] ]},
          psum_spad: {
            num: [4,4],
            dim: [X,Y] }}
        }
      }
    }
  }
}

```

(a) Spatial accelerator description

```

// DRAM to L2
temporal_order : I J K
temporal_tile_sizes : 16, 32, 32
Spatial_tile_size : 16, 32, 32

// V2 to L1
temporal_order : I J K
temporal_tile_sizes : 16, 16, 16
Spatial_tile_size : 4, 4, 4

// L1 to MAC
temporal_order : I J K
temporal_tile_sizes : 4, 4, 4
Spatial_tile_size : 4, 4, 4

// Spatial Dim Info
Space_X: I
Space_Y: J
Simd : K

```

(b) Mapping description

Fig. 3. Example of the spatial architecture description

We target the data file to describe the spatial/temporal tile relations use loop-centric approach like Union [8]. In the mapping abstraction, the meanings of the description notations we used are summarized in Table 2.

TABLE 2
Description of notations used in abstraction for Mapping.

Nation	Description
temporal_ordinal	the temporal ordering between in current memory level
temporal_tile_size	the size of temporal tile for each dimension in current memory level
spatial_tile_size	the size of temporal and spatial tile for each dimension in current memory level
Space_X, Space_Y	the parallelizable dimension map to the physical x and y axes
SIMD	vectorized dimension

To avoid ambiguity, we use Space_X and Space_Y to describe the parallelizable dimension map to the physical x and y axes. After determining the space loop, we need to determine the parallelism of the space loop. We define the k dimension of spatial and temporal tile size in i th level memory as S_i^k, T_i^k , which can be divide into smaller spatial tile size and distributed into multi instances of the level-($i-1$) memory. if $\frac{T_i^k}{S_i^k}$ is greater than one, it means that the k dimension in the level- i memory is parallel, and the parallelism is $\frac{T_i^k}{S_i^k}$. A example mapping for MM operator is shown in Fig.3(b), we notice that $\frac{T_{L1}^I}{S_{L1}^I} = 4$ and $\frac{T_{L1}^J}{S_{L1}^J} = 4$,

which means I, J are parallel, and the parallelism of the I, J dimensions is 4,4, respectively.

Before evaluating the mapping performance, we need to check the legality of the mapping with several rules: (1) the execution order of statement instances must not violate the original statement dependencies. (2)the parallelism for the k dimension at i -level memory, which should be equal to or small then the number of ($i-1$)-level memory. (3)the tile size must meet the hardware specifications and be less than or equal to the capacity of the corresponding memory.

We integrate the mapping description with Schedule Trees [6] to represent the lexicographical order of the workload. The schedule tree starts with a domain node that defines the iteration domain of the program, followed with band nodes that encodes the partial schedule at each loop dimension [9].

```

domain: { S_0[i, j, k] : 0 <= i <= 31 and 0 <= j <= 31 and 0 <= k <= 31 }
mark: kernel
band: [[ S_0[i, j, k] -> [(floor((i)/16))] ]]
mark: L3
band: [[ S_0[i, j, k] -> [(floor((j)/16))] ]]
band: [[ S_0[i, j, k] -> [(floor((k)/4))] ]]
band: [[ S_0[i, j, k] -> [(floor((i)/4) - 4*floor((i)/16)] ] ]
band: [[ S_0[i, j, k] -> [(floor((j)/4) - 4*floor((j)/16)] ] ]
mark: L2
mark: L1
band: [[ S_0[i, j, k] -> [(i mod 4)] ],
      { S_0[i, j, k] -> [(j mod 4)] },
      { S_0[i, j, k] -> [(k mod 4)] } ]

```

Fig. 4. Schedule tree of MM after loop transformation

We construct a schedule tree that includes the memory hierarchy using mapping, as shown in Fig.4. We mark the memory level using **mark** node, indicating that the subtree band is associated with the next level of memory. In addition, we add an attribute of the scheduling tree band to indicate whether the loop is a time loop or a space loop. Due to space limitations, we do not mark it in Fig.4 but marked the space loop band in red color, and the time loop band in black color.

3.2 Data Placement Relation

The major feature of our polyAcc is to capture the runtime behavior of all the physical units in the hardware by data placement relation. Our data placement relation applies an affine function to capture the space-time hierarchy, each (\vec{s}, \vec{t}) pair corresponds to a memory level in the hardware, where \vec{s} and \vec{t} are multi-dimensional vector to describe space-stamp and time-stamp. The \vec{s} describes hardware unit coordinates where statement instances are executed. The \vec{t} determines the execution sequence, a classical lexicographical ordering to realize relative ordering among timestamps when statement instances are executed in the current memory level.

We define *space-time map* of the level- i memory as follows:

$$ST = \{S[\vec{n}] \rightarrow [[\vec{s}] \rightarrow [\vec{t}]]\} \quad (2)$$

The equation 2 denotes that loop instance or loop tile $S[\vec{n}]$ is accessed by hardware unit \vec{s} in the level- i memory at the time-stamp \vec{t} .

We scan the schedule tree from top to bottom, using the time band as the time-stamp vector \vec{t} and the space band as the space-stamp vector \vec{s} for the memory level represented by the mark node; if there is no space band, the space-stamp vector is constant 1. When calculating the affine expression of the time-stamps, the lexicographic order of the loop instances and the inter-unit's connections in the current memory level need to be considered.

We can combine the Access Function \mathbf{R} and space-time map \mathbf{ST} to model the array reference mapping in time-stamp and space-stamp at level- i memory. We define the data placement relation θ of array M of level- i memory:

$$\theta_i^M = \{M[\vec{p}] \rightarrow [[\vec{s}_i] \rightarrow [\vec{t}_i]]\} \quad (3)$$

where \vec{s}_i, \vec{t}_i represent the space-stamps and time-stamps of the i -level memory hardware unit. Equation 3 indicates that array elements $M[\vec{p}]$ appear in i -level memory hardware unit $[\vec{s}_i]$ at time $[\vec{t}_i]$.

Considering the impact of memory in the accelerator, We define the data placement relation Θ to capture the moving relation from $(i+1)$ -level memory to i -level memory:

$$\Theta_i^M = \{M[\vec{p}] \rightarrow [[[\vec{s}_{i+1}] \rightarrow [\vec{t}_{i+1}]] \rightarrow [[\vec{s}_i] \rightarrow [\vec{t}_i]]]\} \quad (4)$$

where s_{i+1}, t_{i+1} and s_i, t_i represent space-stamp and time-stamp of the parent level and child level.

The data placement relation θ provides a relation to data on how to place in space-stamps and time-stamps. For a given mapping, the space-time map ST and the array access function of the workload together can precisely identify what array elements set must appear at each space-time coordinate of each hardware unit.

3.3 Performance model

Based on the data placement relation, we know that when the data is placed in which unit in the memory level. We can precisely compute various performance metrics using the ISL and Barvinok library. Below, we introduce the performance metrics involved in this article, including data reuse, latency, and energy.

3.3.1 Data Reuse and Unique Volume

The memory hierarchies and dataflow of spatial accelerators lead to different data access patterns. Evaluating the mapping for metrics starts with defining several data volumes, including different data reuse volume and unique volume.

1) Data Reuse Volume is the amount of data reuse across multiple time-stamps or space-stamps, including temporal reuse volume (TV), spatial reuse volume (SV) and temporal-spatial reuse volume (TSV).

Algorithm 1 describes the detailed procedure of calculating the data volumes for different access pattern, We derive some R-transfer relations(line 2 - line 4) to exploit data reuse at the current level. R-transfer relations specify a schedule for moving data instance or data tiles from parent unit to child unit. Once R-transfer relations are determined, we derive activity counts representing the workload's execution (eg. TV, SV, TSV).

Algorithm 1 Calculate the data volumes for different access pattern at level - i memory

Input: The DPA of array M in the level- i memory, Θ_i^M ;

Output: The number of temporal reuse volume, TV ;

The number of spatial reuse volume, SV ;

The number of temporal-spatial reuse volume, TSV ;

The number of unique volume, UV ;

The number of total memory access count, $Total$;

1: the DPA is

$$\Theta_i^M = \{M[\vec{p}] \rightarrow [[[\vec{s}_{i+1}] \rightarrow [\vec{t}_{i+1}]] \rightarrow [[\vec{s}_i] \rightarrow [\vec{t}_i]]]\}$$

$$2: R_{_t} = \{[[[\vec{s}_{i+1}] \rightarrow [\vec{t}_{i+1}]] \rightarrow [[\vec{s}_i] \rightarrow [\vec{t}_i]] \rightarrow [[[\vec{s}_{i+1}] \rightarrow [\vec{t}_{i+1}]] \rightarrow [[\vec{s}_i] \rightarrow [\vec{t}_i]]] : \vec{t}_i \ll \vec{t}'_i\}$$

$$3: R_{_s} = \{[[[\vec{s}_{i+1}] \rightarrow [\vec{t}_{i+1}]] \rightarrow [[\vec{s}_i] \rightarrow [\vec{t}_i]] \rightarrow [[[\vec{s}_{i+1}] \rightarrow [\vec{t}_{i+1}]] \rightarrow [[\vec{s}_i] \rightarrow [\vec{t}_i]]] : \vec{s}_{i+1} \ll \vec{s}'_i \wedge \vec{s}_i \gg \vec{s}'_i\}$$

$$4: R_{_st} = \{[[[\vec{s}_{i+1}] \rightarrow [\vec{t}_{i+1}]] \rightarrow [[\vec{s}_i] \rightarrow [\vec{t}_i]] \rightarrow [[[\vec{s}_{i+1}] \rightarrow [\vec{t}_{i+1}]] \rightarrow [[\vec{s}_i] \rightarrow [\vec{t}_i]]] : \vec{t}_i \ll \vec{t}'_{i+1} \wedge ((\vec{s}_i \ll \vec{s}'_i) \vee (\vec{s}_i \gg \vec{s}'_i))\}$$

$$5: \Delta_t = \Theta_i^M \cap (\Theta_i^M \circ R_{_t})$$

$$6: \Delta_s = \Theta_i^M \circ R_{_s}$$

$$7: \Delta_{st} = \Theta_i^M \cap (\Theta_i^M \circ R_{_st})$$

$$8: Total = sum(\Theta_i^M)$$

$$9: TV = sum(\Delta_t)$$

$$10: SV = sum(\Delta_s)$$

$$11: TSV = sum(\Delta_{st})$$

$$12: UV = Total - TSV$$

$$13: \text{return } TV, SV, TSV, UV, Total$$

We use temporal reuse as a example to illustrated how to compute data reuse volume. The R-transfer relations(line 2) about temporal reuse in the level- i memory as follow:

$$R_{_t} = \{[[[\vec{s}_{i+1}] \rightarrow [\vec{t}_{i+1}]] \rightarrow [[\vec{s}_i] \rightarrow [\vec{t}_i]] \rightarrow [[[\vec{s}_{i+1}] \rightarrow [\vec{t}_{i+1}]] \rightarrow [[\vec{s}_i] \rightarrow [\vec{t}_i]]] : \vec{t}_i \ll \vec{t}'_i\} \quad (5)$$

where $\vec{s}_{i+1}, \vec{t}_{i+1}$ and \vec{s}_i, \vec{t}_i represent the space-stamp and time-stamp of the $(i+1)$ -level and i -level memory respectively. The operator \ll represents the closest time vector in their lexicographic orderings.

The level- $(i+1)$ is parent level of and level- i memory, which means the level- i unit \vec{s}_i fetch data from \vec{s}_{i+1} in time \vec{t}_i . $R_{_t}$ takes into account the fact that date was already present in the \vec{s}_i at time \vec{t}_i need not be fetched from anywhere at time \vec{t}_i . We have similar R-transfer relations for other forms of reuse such as spatial reuse and temporal-spatial reuse.

2) Data Unique Volume is the number of unique data at the current memory level. Data is considered unique if it can not fetched from adjacent time-stamps at the same space-stamps. It can be calculated by the difference in DPR of adjacent time-stamps.

3.3.2 Utilization of PE Array

PE array utilization can be computed by dividing the number of active MAC units by the total number of physical MAC units, utilization is only related to spatially unrolled loops.

$$Util = \frac{Total_{mac}}{PE_{size}} \quad (6)$$

3.3.3 Estimating Energy Consumption

The energy consumption is an essential metric for accelerator. We take into account MAC computation energy and memory access energy. For each operator, the total energy is the sum of activate and idle components of MAC, on-chip scratchpad access energy, main memory DRAM access energy and interconnect energy, expressed as follows:

$$E_{total} = E_{mac} + E_{on-chip} + E_{DRAM} + E_{connect} \quad (7)$$

1) Compute Energy. We define MAC computation energy as computing energy consisting of two components: the activate MAC energy and the idle MAC energy. The active energy consumed in performing a MAC operation and idle energy consumed per compute unit when not actively performing a compute operation. Total compute energy is calculated as follows:

$$E_{mac} = (Util \times e_{act} + (1 - Util) \times e_{idle}) \times Total_{mac} \quad (8)$$

where $Util_{PE}$ is utilization of PE array, the $e_{activate}$ is active energy consumed by the MAC per operation, and e_{idle} is energy consumed when MAC is inactive.

2) On-chip scratchpad Energy. On-chip scratchpad energy consists of read energy and write energy as follows:

$$E_{On-chip} = \sum_{op=1}^{operands} e_w \times UV^{op} + e_r \times (UV_{child}^{op} + TV_{child}^{op}) \quad (9)$$

where e_w , e_r are the energy consumed by each write operation and read operation of the on-chip scratchpad, y represent array index. Considering the impact of data reuse, the write energy is the product of e_w and the unique volume (UV); the read energy is the product of e_r and the unique volume (UV), temporal reuse volume (TV) of the child-level memory.

3) Main Memory Energy. We derive the energy consumption of main memory as follows:

$$E_{dram} = \sum_{op=1}^{operands} e_w \times UV^{op} + e_r \times (UV^{op} + TV^{op}) \quad (10)$$

where e_w , e_r are the energy consumed by each write operation and read operation of the DRAM, y represent array index. UV and TV are the unique volume, temporal reuse volume of memory connected to DRAM.

4) Connect Energy. We model the energy consumed by connects that multi-cast connects and inter-connect for each level memory as follows:

$$E_{connect} = \sum_{op=1}^{operands} (e_{multi} \times SV_i^{op} + e_{inter} + TSV_i^{op}) \quad (11)$$

Where e_{multi} and e_{inter} are the energy consumed by multi-cast connects and inter-connect from parent-level memory to child-level memory. The total connect energy consumption is the sum of the per-data-access energy multiplied by the spatial reuse volume SV and the temporal-spatial reuse volume TSV for each memory level.

3.3.4 Execution Time

The execution time of spatial accelerator consists of communication and computation time. We assume accelerator works in a pipeline fashion, the overall execution time is just the maximum of communication time $cycles_{comm}$ and computation time $cycles_{comp}$.

$$total_cycles = \max(cycles_{comp}, cycles_{comm}) \quad (12)$$

1) computation time. The computation time can be estimated by the total number of mac operations and the average number of active PEs, it is calculated as follows:

$$cycles_{comp} = \frac{total_{mac}}{act_{PE}} \times lat_{avg} \quad (13)$$

where $active_{PE}$ is the number of activate PEs across time-stamps, and lat_{avg} is average time of MAC operation.

2) communication time. To model communication time, we takes into account the fact that the data are fetch from DRAM to on-chip scratchpad, then the data in on-chip scratchpad are broadcast to private register files (RF) in PE. The communication time consists of two parts, the time for DMA access to DRAM and the time for data transfer in the on-chip scratchpad.

First, we calculate the time for DMA access to DRAM. The volume of data transferred from the DRAM to the on-chip scratchpad is estimated by the UV of operands; in other words, the total burst size of DMA is UV. To calculate DMA cycles, we consider a latency model of Cell processors [10], i.e.,

$$cycles_{DMA}^{op} = (reqs \times init + 0.25 \times UV_{op}) \times \frac{f_{accel}}{f_{dma}} \quad (14)$$

where $reqs$ is the total DMA invocations required, $init$ is DMA latency, f_{accel} and f_{dma} are the frequencies of the DMA and accelerator respectively. And, we calculate the cycles required for accessing the DRAM as follows:

$$cycles_{DRAM} = \sum_{op=1}^{operands} cycles_{DMA}^{op} \quad (15)$$

Second, we calculate the time for data transfer between the on-chip scratchpad and RFs in PEs. While PEs process data from RFs, if operands are not reused, new data for the next new data tile needs to be fetched from the on-chip scratchpad and communicated to PEs via interconnect. The time for data transfer via the interconnect of PEs and the computation performed by the PE are coincident. Therefore, we consider the time of multicasting or unicasting the data from the on-chip scratchpad to the RF. The cycles required for multicast and unicast operands are respectively:

$$cycles_{multicast}^{op} = \frac{SV}{B} \quad (16)$$

$$cycles_{unicast}^{op} = \frac{\max(Total - SV - TV, 0)}{B} \quad (17)$$

where B is the width of the data bus for interconnect. Total cycles required to transfer data between the on-chip scratchpad and RFs is

$$cycle_{on-chip} = \sum_{op=1}^{operands} cycles_{multicast}^{op} + cycles_{unicast}^{op} \quad (18)$$

Based on the cycles required for accessing the DRAM and the time for data transfer from the scratchpad to RFs, we calculate the total cycles required for communication as follows:

$$cycles_comm = \max(cycles_{DRAM}, cycle_{on-chip}) \quad (19)$$

4 EVALUATION

4.1 Experiment Setup And Analysis

Benchmarks GEMM and 2D-Convolution operator are widely used in deep learning, scientific computations, We evaluate PolyAcc with them, Table 3 list 6 dataflows that we use to evaluate our framework, including corresponding workloads and PE sizes. The dataflow is mainly named according to the spatial loop executed in the space, such as the **(IJ-sp)** data-flow in the GEMM operator, which means that PEs are grouped based on the unrolled I and J loops for spatial execution.

TABLE 3
Operator, Dataflow and PE size used in evaluation

Benchmark	Problem size	dataflow(Sp:Space loop)	PE Size
GEMM	[i,j,k]:[256,256,256]	Output-Satation(IJ-Sp)	8×8
		Weight-Station(KJ-Sp)	8×8
		Vector(J-Sp)	1×64
2D-CONV	AlexNet-conv2 [11]	ROW-Station($O_y O_y - Sp$) [12]	14×12
	MobileNetV2-2 [13]	Weight-Satation(KC-Sp)	8×8
	ResNet50-1 [14]	Shi-dianna($O_x O_y - Sp$) [15]	8×8

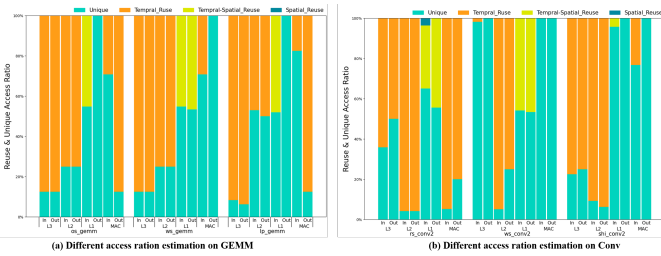


Fig. 5. The result of data access pattern in different dataflow for GEMM and 2D-Conv respectively.

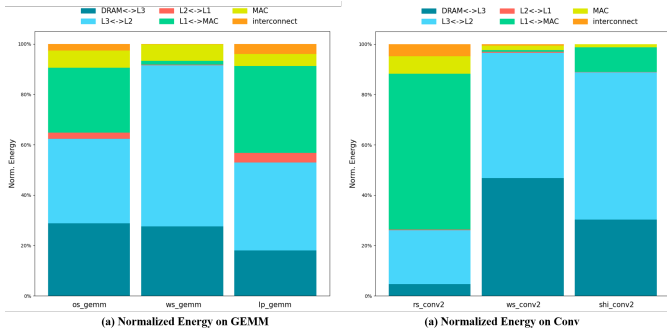


Fig. 6. Energy analysis for GEMM and 2D-Conv, respectively.

Fig.5 shows the data access pattern in different level memory for GEMM and 2D-Conv. We find that different

dataflows have high variation in data access patterns because of the interconnect of PEs in different dataflows. We observe that the data access pattern of each memory level is different. For example, The data access pattern at the L3 level is mainly the temporal reuse since L3-level memory as a data buffer fetches data from DRAM, reducing DRAM access and energy consumption.

Moreover, Fig.6 shows the breakdown of the energy for system resources. It noted that the different colors in the bars represent the energy consumption of different memory levels or interconnects. We observe that the energy consumption is attributed to accessing data from the private/shared scratchpad, and the unique access of the child memory level affects the energy consumption of data access at the parent memory level. For optimized the execution of workloads on the spatial accelerator, the dedicated memory resources should be fully utilized for data reuse as much as possible, reducing the energy consumption of unique accessing.

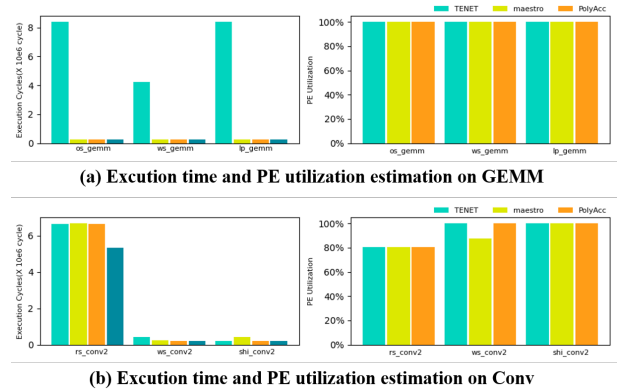


Fig. 7. Execution time and PE utilization comparison with MAESTRO and TENET. (a) and (b) are the result of execution time and PE utilization for GEMM and 2D-Conv, respectively. (Right: Execution time; Left: PE utilization)

Fig.7 compares the execution time and PE utilization of TENET and MASTERO on our benchmarks. We approximate the ground-truth value of execution time for estimated execution time using $\frac{totalMACOperations}{totalPEs}$. Furthermore, we find that our estimations closely matched the execution time of the ideal value. For estimated execution time, The estimated results of the three frameworks are similar, with a difference of 12.5% in the largest.

4.2 Estimation Comparison

We comparison our framework with the recent work [4], [5], which are the state-of-the-art relation-centric and data-centric notation with comprehensive performance analysis. We show that our proposed model improves the metric estimation accuracy.

We considered a similar dataflow accelerator architecture as [12], which consists of 14×12 PEs with 16-bit precision, and it has two levels of physical memory(global buffer and register file inside the PE) and one level of virtual memory that model NOC, the multi-cast networks to communicate the operands to PEs. We configure the them to use the same parameters (PE Number, Bandwidth, Buffer Size). For the interconnection parameters of PolyAcc, We define the

connection relationship of the output feature downward, the weight to the left, and the input feature multicast communication along the diagonal line, respectively.

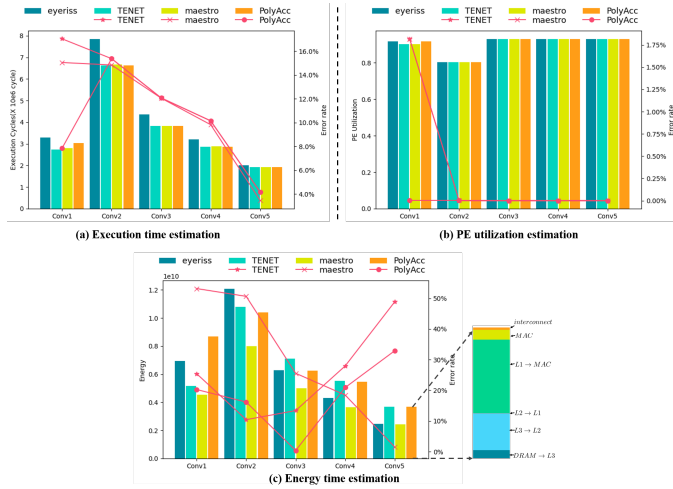


Fig. 8. Latency, Energy, and PE utilization comparison with TENET and MAESTRO. (a), (b) and (c) are the result of Eyeriss-like [12] accelerator running AlexNet [11]. Conv1-Conv5 means convolutional layer in Alexnet.

We compare the execution time, PE utilization and energy calculated by our work and TENET, MAESTRO. Fig.8 shows the comparison results. PolyAcc achieves the same PE utilization as Yang as eyeriss and TENET. Moreover, for various mapping mechanisms, the execution time estimated by PolyAcc closely matched execution cycles of the accelerator [12] thanks to more accurate reuse analysis, the difference is from 4.15% to 15.4%. Furthermore, We entirely consider the energy cost of the different data access patterns in different memory levels, which supports calculate the energy of different memory level. The result shows that the energy estimated by PolyAcc closely matched the [12], with a difference of 7.5% in the energy consumption.

5 CONCLUSION

In this work, we propose PolyAcc evaluate the performance of workload mappings on spatial accelerators. We present analysis methods leverage data placement, which can accurately capture the runtime behavior of hardware units. We evaluate our framework on six benchmarks, and results show that polyAcc closely matched the ideal value's execution time and PE utilization. On validation against Eyeriss architecture, PolyAcc achieves 0.82% improvements in execution time and 18.8% improvements in energy consumption estimates compared to the state-of-the-art framework thanks to sophisticated data reuse analysis.

REFERENCES

- [1] A. Parashar, P. Raina, Y. S. Shao, Y.-H. Chen, V. A. Ying, A. Mukkara, R. Venkatesan, B. Khailany, S. W. Keckler, and J. Emer, "Timeloop: A systematic approach to dnn accelerator evaluation," in *2019 IEEE International Symposium on Performance Analysis of Systems and Software (ISPASS)*, 2019, pp. 304–315.
- [2] X. Yang, M. Gao, Q. Liu, J. Setter, J. Pu, A. Nayak, S. Bell, K. Cao, H. Ha, P. Raina, C. Kozyrakis, and M. Horowitz, *Interstellar: Using Halide's Scheduling Language to Analyze DNN Accelerators*, 2020, p. 369–383.

- [3] S. Dave, Y. Kim, S. Avancha, K. Lee, and A. Shrivastava, "Dmazerunner: Executing perfectly nested loops on dataflow accelerators," *ACM Trans. Embed. Comput. Syst.*, vol. 18, no. 5s, oct 2019.
- [4] H. Kwon, P. Chatarasi, M. Pellauer, A. Parashar, V. Sarkar, and T. Krishna, "Understanding reuse, performance, and hardware cost of dnn dataflow: A data-centric approach," ser. MICRO '52, 2019, p. 754–768.
- [5] L. Lu, N. Guan, Y. Wang, L. Jia, Z. Luo, J. Yin, J. Cong, and Y. Liang, "Tenet: A framework for modeling tensor dataflow based on relation-centric notation," in *2021 ACM/IEEE 48th Annual International Symposium on Computer Architecture (ISCA)*, 2021, pp. 720–733.
- [6] S. Verdoolaege, S. Guelton, T. Grosser, and A. Cohen, "Schedule trees," 01 2014.
- [7] S. Verdoolaege, "isl: An integer set library for the polyhedral model," in *Mathematical Software – ICMS 2010*, K. Fukuda, J. v. d. Hoeven, M. Joswig, and N. Takayama, Eds., 2010, pp. 299–302.
- [8] G. Jeong, G. Kestor, P. Chatarasi, A. Parashar, P.-A. Tsai, S. Rajamanickam, R. Gioiosa, and T. Krishna, "Union: A unified hw-sw co-design ecosystem in mlir for evaluating tensor operations on spatial accelerators," in *2021 30th International Conference on Parallel Architectures and Compilation Techniques (PACT)*, 2021, pp. 30–44.
- [9] J. Wang, L. Guo, and J. Cong, "Autosa: A polyhedral compiler for high-performance systolic arrays on fpga," in *The 2021 ACM/SIGDA International Symposium on Field-Programmable Gate Arrays*, ser. FPGA '21, 2021, p. 93–104.
- [10] M. Kistler, M. Perrone, and F. Petrini, "Cell multiprocessor communication network: Built for speed," *IEEE Micro*, vol. 26, no. 3, pp. 10–23, 2006.
- [11] A. Krizhevsky, I. Sutskever, and G. E. Hinton, "Imagenet classification with deep convolutional neural networks," *Commun. ACM*, vol. 60, no. 6, pp. 84–90, 2017.
- [12] Y.-H. Chen, T. Krishna, J. Emer, and V. Sze, "Eyeriss: An energy-efficient reconfigurable accelerator for deep convolutional neural networks," in *2016 IEEE International Solid-State Circuits Conference (ISSCC)*, 2016, pp. 262–263.
- [13] M. Sandler, A. G. Howard, M. Zhu, A. Zhmoginov, and L. Chen, "Mobilenetv2: Inverted residuals and linear bottlenecks," in *2018 IEEE Conference on Computer Vision and Pattern Recognition, CVPR 2018, Salt Lake City, UT, USA, June 18–22, 2018*. Computer Vision Foundation / IEEE Computer Society, 2018, pp. 4510–4520.
- [14] K. He, X. Zhang, S. Ren, and J. Sun, "Deep residual learning for image recognition," in *2016 IEEE Conference on Computer Vision and Pattern Recognition, CVPR 2016, Las Vegas, NV, USA, June 27–30, 2016*. IEEE Computer Society, 2016, pp. 770–778.
- [15] Z. Du, R. Fasthuber, T. Chen, P. Ienne, L. Li, T. Luo, X. Feng, Y. Chen, and O. Temam, "Shidiannao: shifting vision processing closer to the sensor," in *Proceedings of the 42nd Annual International Symposium on Computer Architecture*, D. T. Marr and D. H. Albonesi, Eds., 2015, pp. 92–104.